

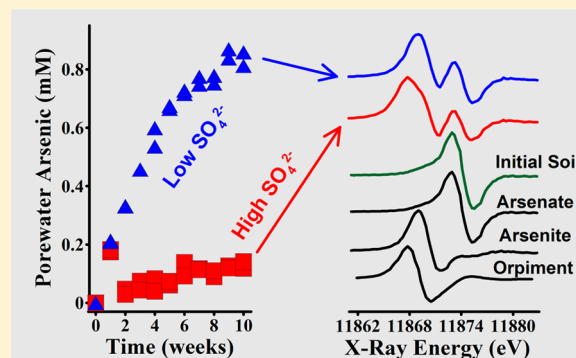
## Arsenic Mobility during Flooding of Contaminated Soil: The Effect of Microbial Sulfate Reduction

Edward D. Burton,<sup>\*,†</sup> Scott G. Johnston,<sup>†</sup> and Benjamin D. Kocar<sup>‡</sup>

<sup>†</sup>Southern Cross GeoScience, Southern Cross University, Lismore, NSW 2480, Australia

<sup>‡</sup>Department of Civil and Environmental Engineering, Massachusetts Institute of Technology, Cambridge, Massachusetts 02139, United States

**ABSTRACT:** In floodplain soils, As may be released during flooding-induced soil anoxia, with the degree of mobilization being affected by microbial redox processes such as the reduction of As(V), Fe(III), and SO<sub>4</sub><sup>2-</sup>. Microbial SO<sub>4</sub><sup>2-</sup> reduction may affect both Fe and As cycling, but the processes involved and their ultimate consequences on As mobility are not well understood. Here, we examine the effect of microbial SO<sub>4</sub><sup>2-</sup> reduction on solution dynamics and solid-phase speciation of As during flooding of an As-contaminated soil. In the absence of significant levels of microbial SO<sub>4</sub><sup>2-</sup> reduction, flooding caused increased Fe(II) and As(III) concentrations over a 10 week period, which is consistent with microbial Fe(III)- and As(V)-reduction. Microbial SO<sub>4</sub><sup>2-</sup> reduction leads to lower concentrations of porewater Fe(II) as a result of FeS formation. Scanning electron microscopy with energy dispersive X-ray fluorescence spectroscopy revealed that the newly formed FeS sequestered substantial amounts of As. Bulk and microfocused As K-edge X-ray absorption near-edge structure spectroscopy confirmed that As(V) was reduced to As(III) and showed that in the presence of FeS, solid-phase As was retained partly via the formation of an As<sub>2</sub>S<sub>3</sub>-like species. High resolution transmission electron microscopy suggested that this was due to As retention as an As<sub>2</sub>S<sub>3</sub>-like complex associated with mackinawite (tetragonal FeS) rather than as a discrete As<sub>2</sub>S<sub>3</sub> phase. This study shows that mackinawite formation in contaminated floodplain soil can help mitigate the extent of arsenic mobilization during prolonged flooding.



### INTRODUCTION

Arsenic is a commonly encountered contaminant in floodplain environments because of its release during industrial, mining, and agricultural activities.<sup>1</sup> The toxicity and mobility of arsenic in soil environments is a function of its oxidation state and its sorption to soil minerals and organic matter.<sup>2</sup> Under well-aerated (oxic) soil conditions, As exists primarily in its As(V) oxidation state as the arsenate oxyanion (HAsO<sub>4</sub><sup>2-</sup>, H<sub>2</sub>AsO<sub>4</sub><sup>-</sup>). Arsenate interacts strongly with Fe(III) oxyhydr(oxide) minerals, with this group of minerals being important sorbents for As(V) in oxic soils.<sup>3</sup>

When oxic soils are flooded, microbial consumption of O<sub>2</sub> can lead to the development of anoxic conditions. Several studies have shown that porewater As concentrations often increase following flooding-induced soil anoxia.<sup>4–7</sup> This increase in porewater As has been attributed to two dominant processes. First, some anaerobic microorganisms are capable of reducing As(V) to more mobile As(III).<sup>8</sup> Second, Fe(III) oxyhydr(oxide)s, which are powerful sorbents of As(V) and As(III),<sup>2</sup> can undergo reductive dissolution through the activity of dissimilatory Fe(III)-reducing microorganisms. Dissolution of Fe(III) oxyhydr(oxide)s results in a loss of sorption sites and the release of previously sorbed As.<sup>2</sup>

Arsenic behavior in anoxic soils and sediments may also be affected by microbial SO<sub>4</sub><sup>2-</sup> reduction.<sup>9–15</sup> Microbially produced sulfide can reduce both Fe(III) and As(V), which thereby drives As release into the aqueous phase.<sup>16,17</sup> Alternatively, under different conditions, sulfide can immobilize As by facilitating the precipitation of As sulfide and Fe sulfide minerals.<sup>5,11,18–21</sup> While As sulfide precipitation obviously removes As from solution, the efficacy of As sorption to Fe sulfides is complex and difficult to predict. This is because the extent and strength of As sorption to Fe sulfides can vary widely, depending on aqueous As speciation, pH, and iron sulfide mineralogy.<sup>22–27</sup>

Microbial SO<sub>4</sub><sup>2-</sup> reduction can hypothetically induce As mobilization or retention in flooded soil, depending on the dominating operative processes mentioned above. However, our present understanding of these processes and their magnitude in natural soils is insufficient to predict the overall effect of microbial sulfate reduction on As mobility. Therefore, the purpose of this study was to help constrain our

Received: August 13, 2014

Revised: October 22, 2014

Accepted: October 26, 2014

Published: October 26, 2014

understanding of the effect of microbial  $\text{SO}_4^{2-}$  reduction on arsenic speciation and partitioning during inundation of As-contaminated soil.

## EXPERIMENTAL SECTION

**Soil Sampling and Characterization.** Approximately 50 kg of soil was collected from the surface layer (0–10 cm) of a gleyic fluvisol on a floodplain of the Tweed River, eastern Australia. The sampling site was agricultural land, where arsenical compounds were used to treat tick infestations in cattle during the 1950s. In eastern Australia, soil As concentrations of up 3000 mg kg<sup>-1</sup> are common at such sites due to use of As-based pesticides during the early to mid-1900s.<sup>28</sup> At the time of sampling, the surface horizon was unsaturated and well-aerated. After collection, the soil material was air-dried and passed through a 2 mm sieve before being stored in plastic containers in the dark.

**Soil Flooding Experiment.** The effect of microbial sulfate reduction was examined by a series of anoxic soil/water incubation experiments employing three contrasting levels of  $\text{SO}_4^{2-}$  availability under the influence of microbial activity or under abiotic conditions. Ten grams of air-dry soil was weighed into a series of 50 mL polypropylene vials. Each vial then received 40 mL of water containing 0, 2, or 20 mM  $\text{Na}_2\text{SO}_4$ , denoted as low, medium, and high  $\text{SO}_4^{2-}$  treatments, respectively. The low, medium, and high  $\text{SO}_4^{2-}$  treatments also received 40, 36, or 0 mM NaCl to ensure comparable ionic strength between treatments. For each of the three  $\text{SO}_4^{2-}$  treatments, additional vials also received 20 mM  $\text{NaN}_3$  to inhibit microbial activity. Those vials that received  $\text{NaN}_3$  are herein termed abiotic treatments, and those that did not receive  $\text{NaN}_3$  are termed biotic treatments.

The soil/solution microcosms were then transferred (within open 50 mL vials) into a Coy anaerobic chamber containing an O<sub>2</sub>-free atmosphere of 97–98% N<sub>2</sub> and 2–3% H<sub>2</sub> (the chamber contained Pd-catalyst packs that maintained strictly O<sub>2</sub> conditions; verified by monitoring with an O<sub>2</sub> meter). The headspace in the open vials was deoxygenated via equilibration with the O<sub>2</sub>-free atmosphere for 16 h. This 16 h period was sufficient to yield dissolved O<sub>2</sub> concentrations of <0.01 mg L<sup>-1</sup> in the Biotic treatments. The vials were then fitted with gastight screw caps and were allowed to incubate within the anaerobic chamber at room temperature (20 ± 1 °C), with regular shaking, for up to 10 weeks.

Duplicate microcosms were sacrificed for analysis at 1 week intervals over a 10 week period. At each sampling time, the vials were centrifuged at 4000 rpm for 10 min, and the supernatant solution was withdrawn and filtered to <0.2 μm. After removal of the aqueous-phase, the solid-phase was dried under O<sub>2</sub>-free conditions within an anaerobic chamber, finely ground, and stored within butyl-rubber sealed glass vials. All sample processing and storage was completed within an anaerobic chamber under strictly O<sub>2</sub>-free conditions.

**Analytical Methods.** Filtered porewater samples from duplicate reactors collected at each sampling time were analyzed for pH, Eh, H<sub>2</sub>S,  $\text{SO}_4^{2-}$ , total Fe, total As, Fe(II), and As(III) using standard methods as described previously.<sup>15</sup> Soluble and adsorbed As values were determined via extraction with a 1 M phosphate solution.<sup>9</sup> Soil residue remaining after the  $\text{PO}_4^{3-}$  extraction step was subjected to an ascorbate extraction.<sup>29</sup> Together, this two-step extraction scheme targets (1) adsorbed and readily soluble As and (2) As that is associated with easily reducible Fe(III) oxyhydr(oxides)

minerals, respectively. The total As, C, Fe, and S contents were determined as described previously.<sup>4</sup>

The speciation of arsenic in solid-phase samples collected over the incubation experiment was examined by bulk K-edge X-ray absorption near-edge structure (XANES) spectroscopy at the Australian Synchrotron. Details on the experimental setup, data extraction, and determination of bulk As speciation by linear combination fitting have been described previously.<sup>21</sup> Synchrotron-based X-ray microprobe measurements of element distributions were collected at the Stanford Synchrotron Radiation Lightsource (SSRL, SLAC National Accelerator Laboratory, Menlo Park, CA). Solid-phase samples were transported to the SSRL in O<sub>2</sub>-free serum vials with butyl-rubber seals. At the SSRL, a small part of the subsample was dusted onto Scotch tape and placed in a sample holder that was sealed with Mylar film (with all sample preparation conducted under strictly O<sub>2</sub>-free conditions in an anaerobic chamber). Microprobe XRF mapping was performed at beamline 2–3, equipped with a Si(110) double-crystal monochromator and a Vortex fluorescence detector. During X-ray analysis, the sample holder was purged with He to prevent sample oxidation. The spot size was ~2 μm × 2 μm, and XRF maps were collected at 12 000 eV with a dwell time of 25 ms. After mapping, selected spots were targeted for the collection of microfocused As K-edge XANES spectroscopy in fluorescence mode. The ATHENA program was used for standard background subtraction and edge-height normalization.<sup>30</sup>

Samples for scanning electron microscopy (SEM) examination were mounted on aluminum stubs, coated with carbon, and the morphology and elemental composition of solid-phase products determined using a Leica 440 SEM with an ISIS energy dispersive X-ray (EDX) microanalysis system. Samples for transmission electron microscopy (TEM) were prepared by suspending dried powder in ethanol, and drops of the suspension were added onto holey carbon support films. High-resolution TEM (HRTEM), analytical electron microscopy (AEM), and high-angle annular dark-field scanning TEM (HAADF-STEM) was carried out using a JEOL JEM2100F equipped with a thin-window EDX system.

## RESULTS

**Characterization of the Oxic Soil.** The initial oxic soil had a silty-loam texture, was slightly acidic (pH 5.7), and contained  $3.2 \pm 0.1\%$  organic C. It contained  $10.7 \pm 0.2 \mu\text{mol g}^{-1}$  total S,  $758 \pm 21 \mu\text{mol g}^{-1}$  total Fe, and  $20.6 \pm 0.2 \mu\text{mol g}^{-1}$  total As. Of the total Fe content, 34% was present as HCl-extractable Fe(III) ( $260 \pm 4 \mu\text{mol g}^{-1}$ ), with negligible HCl-extractable Fe(II). Approximately 70% of the total As content was extractable by 1 M  $\text{PO}_4^{3-}$ , with the remaining 30% being almost completely recovered by a buffered ascorbic acid extraction. Arsenic XANES spectroscopy indicated that As initially present in the soil existed in the As(V) oxidation state.

**Solution Dynamics.** Figure 1 shows the evolution of porewater pH, Eh,  $\text{SO}_4^{2-}$ , Fe, and As over time. Sulfide concentrations remained below detection (<1 μM) for the full experiment duration and are not presented. Under Abiotic conditions, pH remained close to 5.7 and Eh close to 230 mV for all  $\text{SO}_4^{2-}$  treatments (Figure 1a,b). Under biotic conditions, pH increased toward 6.5 over the initial 5 weeks, and Eh decreased toward 0 mV.

Porewater  $\text{SO}_4^{2-}$  concentrations remained constant under abiotic conditions, with close to 0.6, 2, and 18 mM in the low, medium, and high  $\text{SO}_4^{2-}$  treatments, respectively (Figure 1c).

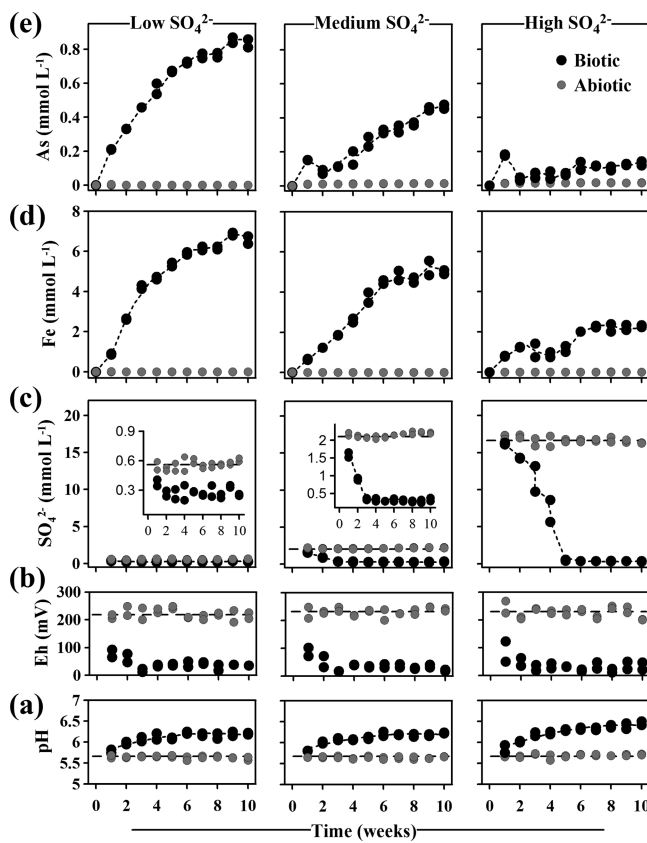


**Figure 1.** Evolution of aqueous-phase composition in the low, medium, and high  $\text{SO}_4^{2-}$  treatment under abiotic versus biotic conditions (from duplicate reactors sacrificed at each time point). The initial solutions used in the low, medium, and high  $\text{SO}_4^{2-}$  treatment contained 0, 2, or 20 mM  $\text{SO}_4^{2-}$ , respectively.

Although the low  $\text{SO}_4^{2-}$  treatment did not receive additional  $\text{SO}_4^{2-}$ , the presence of  $\sim 0.6$  mM porewater  $\text{SO}_4^{2-}$  in this treatment is attributable to dissolution of  $\sim 22\%$  of the soil's native S content. Similar porewater  $\text{SO}_4^{2-}$  concentrations occurred in both the abiotic and biotic treatments at 1 week for each of the respective  $\text{SO}_4^{2-}$  treatments. However, under biotic conditions, porewater  $\text{SO}_4^{2-}$  concentrations began to decrease substantially following week one. In the medium  $\text{SO}_4^{2-}$  treatment, porewater  $\text{SO}_4^{2-}$  decreased from approximately 1.6 mM at week one to  $< 0.1$  mM at week three. In the high  $\text{SO}_4^{2-}$  treatment, porewater  $\text{SO}_4^{2-}$  decreased to  $< 0.1$  mM by week five (Figure 1).

Under abiotic conditions, porewater Fe was present at very low concentrations (Figure 1d). In contrast, relatively high concentrations of Fe were released under biotic conditions, with this Fe existing as  $\text{Fe}^{2+}$ . Over the first week, the release of  $\text{Fe}^{2+}$  was very similar between the different  $\text{SO}_4^{2-}$  treatments, with concentrations at 1 week being  $\sim 1$  mM. In the low  $\text{SO}_4^{2-}$  treatment, porewater  $\text{Fe}^{2+}$  increased over the full experiment duration and reached up to  $\sim 7$  mM (equating to dissolution of  $\sim 10\%$  of initial solid-phase pool of HCl-extractable Fe). In the medium  $\text{SO}_4^{2-}$  treatment, porewater  $\text{Fe}^{2+}$  also increased over time and reached  $\sim 5$  mM at week 10.

In the high  $\text{SO}_4^{2-}$  treatment, there was an initial increase in porewater  $\text{Fe}^{2+}$  over the first 2 weeks as also observed for the low and medium  $\text{SO}_4^{2-}$  treatments (Figure 1d). This initial increase was followed by a slight decrease between week two and week four, which coincided with removal of porewater

$\text{SO}_4^{2-}$ . From week four, porewater  $\text{Fe}^{2+}$  in the high  $\text{SO}_4^{2-}$  treatment began to increase and reached concentrations of 2–3 mM by week seven. This increase in porewater  $\text{Fe}^{2+}$  followed the complete consumption of  $\text{SO}_4^{2-}$  by week five.

Relatively small concentrations of As were released to the porewater under abiotic conditions, with maximum concentrations of  $\sim 0.01$  mM across all  $\text{SO}_4^{2-}$  treatments (Figure 1e). This similarity in porewater As concentrations indicates that aqueous  $\text{SO}_4^{2-}$  had a negligible effect on the abiotic desorption of As(V). In contrast to the low level of abiotic As release, relatively high concentrations of As were mobilized into the porewater under biotic conditions. Hydride-generation atomic absorption spectroscopy (AAS)-based speciation analysis indicated that greater than 90% of porewater As in all biotic treatments was present as As(III) (data not shown).

Over the first week, the extent of As release under biotic conditions was very similar in the low, medium, and high  $\text{SO}_4^{2-}$  treatments (Figure 1e). For example, all three  $\text{SO}_4^{2-}$  treatments displayed porewater As concentrations at week one that were close to  $\sim 0.2$  mM. However, as the experiment progressed, porewater As began to differ between the  $\text{SO}_4^{2-}$  treatments. In the low  $\text{SO}_4^{2-}$  treatment, porewater As continued to increase over the full 10 week duration and reached up to 0.9 mM. These very high porewater As concentrations equate to dissolution of  $\sim 17\%$  of the soil's total As content.

In both the medium and high  $\text{SO}_4^{2-}$  treatments, porewater As concentrations decreased between week one and week two (Figure 1e). This decrease in porewater As coincided with the simultaneous removal of porewater  $\text{SO}_4^{2-}$  and decreases in porewater  $\text{Fe}^{2+}$ . In the medium  $\text{SO}_4^{2-}$  treatment, porewater As increased steadily from week two, with concentrations reaching  $\sim 0.5$  mM by week 10. Porewater As concentrations also increased from week two to week 10 in the high  $\text{SO}_4^{2-}$  treatment. However, the degree of this increase in porewater As was relatively low, with final concentrations of only  $\sim 0.15$  mM at week 10 (i.e., dissolution of only  $\sim 3\%$  of the soil's total As content).

**Solid-Phase Iron and Arsenic Speciation.** Figure 2 presents the first-derivative of As K-edge XANES spectra for solid-phase samples from the biotic low, medium, and high  $\text{SO}_4^{2-}$  treatments compared to selected reference standards. From a qualitative perspective, the XANES spectra indicate the presence of three distinct forms of arsenic within the biotic flooded soil: As(V)–O, As(III)–O, and an As–S species. Inclusion of orpiment ( $\text{As}_2\text{S}_3$ ) as a reference species provided better linear combination fits than did the use of other As–S species, such as realgar (AsS) or arsenopyrite (FeAsS). It should be noted that AsS-like and FeAsS-like species exhibit peak XANES absorbances at lower X-ray energies than that of  $\text{As}_2\text{S}_3$ .<sup>20</sup>

Linear combination fitting of the As K-edge XANES spectra indicates substantial, although incomplete, reduction of As(V) to As(III) during soil flooding (Figure 3). The rates and ultimate extent of As(V) reduction were similar across the three  $\text{SO}_4^{2-}$  treatments, with between 25% and 35% of solid-phase As remaining as As(V) at week 10. In the low and medium  $\text{SO}_4^{2-}$  treatments, the final solid-phase As speciation was dominated by As(III), with either no or very low amounts of an  $\text{As}_2\text{S}_3$ -like As species. As(III) was also the most abundant solid-phase species at week 10 in the high  $\text{SO}_4^{2-}$  treatment. However, in this treatment, an  $\text{As}_2\text{S}_3$ -like As species made up  $\sim 25\%$  of solid-phase As by week 10. It should be noted that the XANES results indicate the development of an  $\text{As}_2\text{S}_3$ -like local

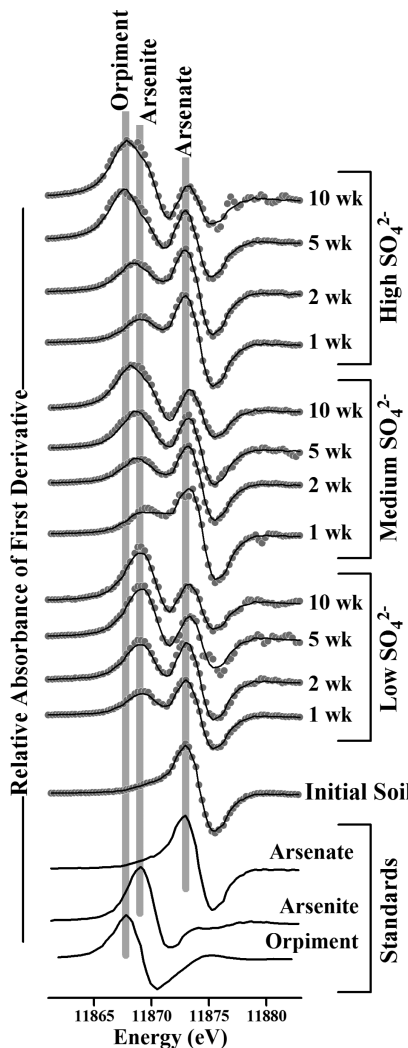


**Figure 2.** First derivative As K-edge XANES spectra for the low, medium, and high  $\text{SO}_4^{2-}$  treatments over time compared to selected reference standards. Symbols denote data points, while the solid line shows the linear combination fit.

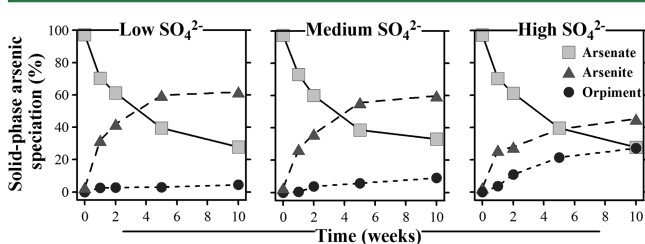


**Figure 3.** Changes over time in solid-phase arsenic speciation based on linear combination fitting of As K-edge XANES data.

coordination environment and not necessarily the presence of a distinct  $\text{As}_2\text{S}_3$  phase.

Figure 4, panel (a) shows the microscale codistribution of As and Fe in material collected at week 10 from the biotic high sulfate treatment. Comparison of As versus Fe fluorescence reveals the existence of multiple, distinct correlations between the two elements (Figure 4b). On the basis of these relationships, we selected four spots for microfocused As K-edge XANES spectroscopy. Spots 2, 3, and 4 exhibited moderate enrichment of As relative to Fe and were found to

contain a mixture of As(III)-O and As(V)-O species (Figure 4c). In contrast, Spot 1 showed very strong enrichment of As relative to Fe and contained As predominantly as an  $\text{As}_2\text{S}_3$ -like species.

Electron microscopy revealed the presence of FeS particles in the biotic high  $\text{SO}_4^{2-}$  treatment at week 10 (e.g., Figures 5 and 6). TEM with selected area electron diffraction (SAED) revealed that the FeS that formed in the biotic high  $\text{SO}_4^{2-}$  treatment exhibited lattice spacings that were consistent with mackinawite, tetragonal FeS (Figure 6). Despite an extensive electron microscopic search, we found no evidence for the presence of other iron sulfides, such as pyrite, or the presence of any discrete As sulfide minerals.

EDX analysis of the mackinawite particles that formed in the biotic high  $\text{SO}_4^{2-}$  treatment revealed a consistent enrichment in As (Figure 5). HAADF-STEM demonstrates that the mackinawite-associated As was homogeneously distributed on/within the mackinawite particles as opposed to existing as discrete As sulfide solids (Figure 6). This shows that, within the biotic high-sulfate treatment, soil flooding led to sorption of As to the newly formed mackinawite.

## DISCUSSION

The soil–water system considered in this study initially contained 2.6 mmol of reactive Fe(III) (based on extraction with 1 M HCl) and 0.02 mmol of As(V) with either ~0.02, ~0.08, or ~0.8 mmol of porewater  $\text{SO}_4^{2-}$  in the low, medium, and high  $\text{SO}_4^{2-}$  treatments, respectively. Therefore, a large excess of reactive Fe(III) relative to both As(V) and  $\text{SO}_4^{2-}$  occurred in all treatments (even in the high  $\text{SO}_4^{2-}$  treatment). The abundance of reactive Fe(III) is reflected in the development of millimolar porewater  $\text{Fe}^{2+}$  concentrations in the biotic treatments. This can be attributed to the microbially mediated reductive dissolution of Fe(III) oxyhydroxides present in the initial oxic soil, a process which would have also released alkalinity and thereby may have driven the observed increase in pH.<sup>15</sup>

The As XANES data shows that As(V) reduction also occurred along with Fe(III) reduction during the initial stages of the experiment. In the low  $\text{SO}_4^{2-}$  treatment, co-occurrence of As(V) reduction and Fe(III) reduction was associated with mobilization of very high concentrations of porewater As. Although there was much less As mobilization in the higher  $\text{SO}_4^{2-}$  treatments, porewater As still reached concentrations that greatly exceeded safe drinking water criteria. For example, the final porewater As concentrations in the high  $\text{SO}_4^{2-}$  treatment were approximately 1000-fold higher than the USEPA's maximum contaminant level of 10  $\mu\text{g L}^{-1}$  in drinking water.<sup>31</sup>

The observed decreases in porewater  $\text{SO}_4^{2-}$  within the biotic treatments can be attributed to microbial  $\text{SO}_4^{2-}$  reduction. Although  $\text{H}_2\text{S}$  is produced by microbial  $\text{SO}_4^{2-}$  reduction, porewater  $\text{H}_2\text{S}$  would have been rapidly consumed via precipitation of mackinawite as a result of excess porewater  $\text{Fe}^{2+}$ . This is consistent with the fact that porewater  $\text{H}_2\text{S}$  remained undetectable throughout the whole experiment. The absence of porewater  $\text{H}_2\text{S}$  due to buffering by abundant  $\text{Fe}^{2+}$  is significant because it indicates that porewater thioarsenic species were likely to have been of negligible importance in the experiment described here.

The observed decrease from week one to week two in porewater As concentrations within the medium and high  $\text{SO}_4^{2-}$  treatments coincided with the onset of microbial  $\text{SO}_4^{2-}$

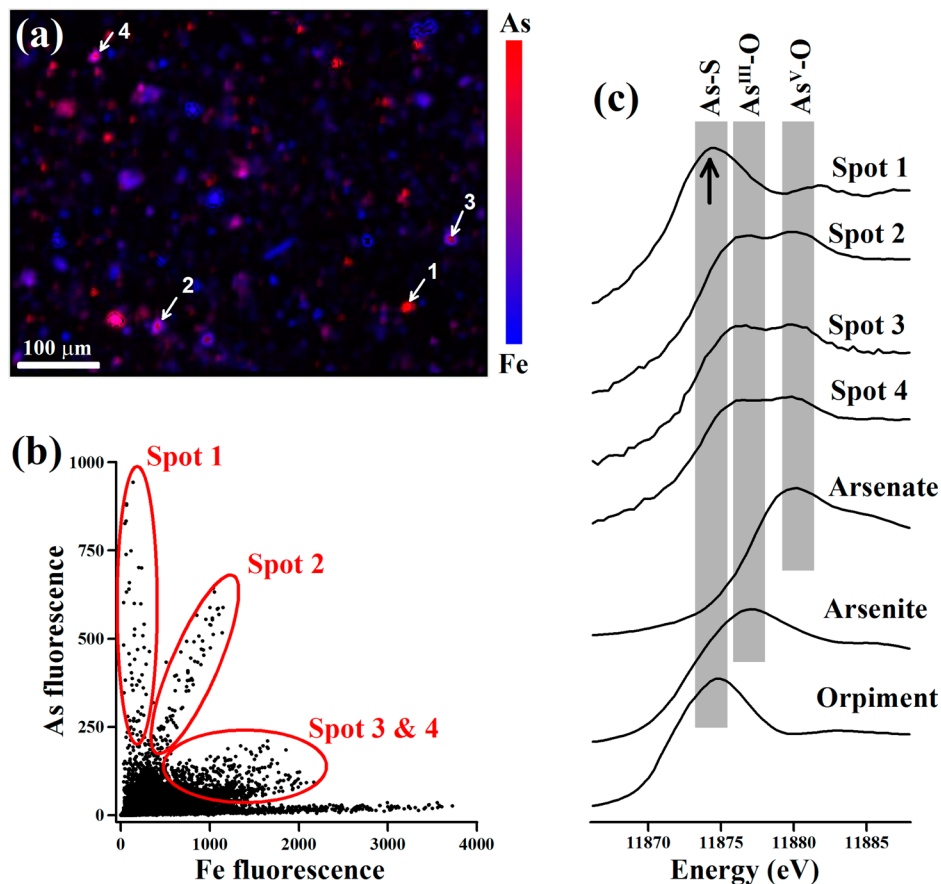


**Figure 4.** (a) Micro-X-ray fluorescence map showing the codistribution of As and Fe in material collected at week 10 from the biotic high sulfate treatment; (b) relationship between microscale As and Fe fluorescence revealing distinct clusters indicated as Spots 1, 2, 3, and 4, which are also marked on the As–Fe map; and (c) normalized As K-edge XANES spectra for points-of-interest in comparison to the corresponding spectra of selected reference standards.

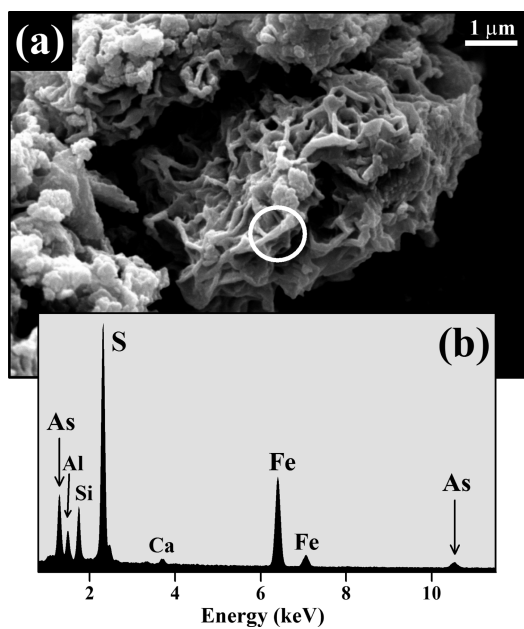


**Figure 5.** (a) Scanning electron micrograph and (b) EDX spectra showing an As-bearing FeS particle formed after 10 weeks in the biotic high  $\text{SO}_4^{2-}$  treatment (initial  $\text{SO}_4^{2-} = 20 \text{ mM}$ ).

reduction. Furthermore, greater extents of microbial  $\text{SO}_4^{2-}$  reduction in the medium and high  $\text{SO}_4^{2-}$  treatments resulted in

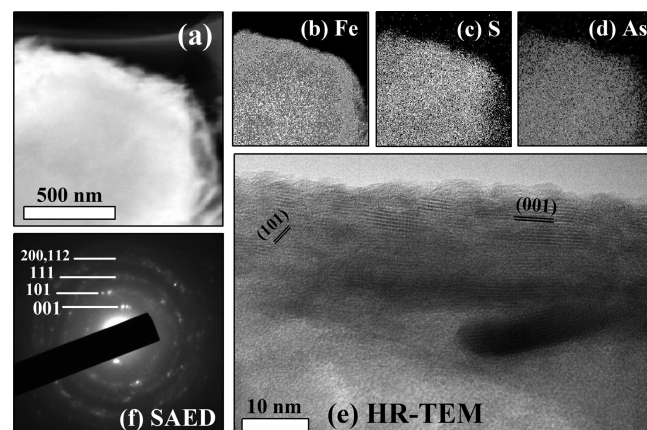


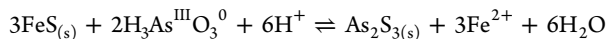
**Figure 6.** Nanoscale As distribution in mackinawite (tetragonal FeS) formed in the biotic high  $\text{SO}_4^{2-}$  treatment (initial  $\text{SO}_4^{2-} = 20 \text{ mM}$ ) after 10 weeks of soil inundation. (a) HAADF-STEM of an FeS particle with EDX mapping of (b) Fe, (c) S, and (d) As; (e) HR-TEM image and (f) SAED pattern of material presented in panel (a) showing lattice fringes, which indicate the presence of mackinawite.

much lower levels of As mobilization in comparison to the low  $\text{SO}_4^{2-}$  treatment. This demonstrates that microbial  $\text{SO}_4^{2-}$  reduction led to the immobilization of a portion of As that would have otherwise been released into solution. From this perspective, it appears that microbial  $\text{SO}_4^{2-}$  reduction under

$\text{Fe}^{2+}$ -rich conditions can help to mitigate As mobility in flooded soil.

Microbial  $\text{SO}_4^{2-}$  reduction may lead to decreased As mobility via a range of possible pathways. First, As can form complexes with organic thiol groups ( $\text{C}-\text{SH}$ ) formed via a reaction between microbially-produced  $\text{H}_2\text{S}$  and soil organic matter. For example, Couture et al.<sup>32</sup> found that microbial  $\text{SO}_4^{2-}$  reduction in sediments with approximately 50% organic matter caused organic matter sulfurization, which subsequently led to formation of solid-phase As–thiol complexes. Importantly, the previous reports of As–thiol complexation are from systems with very low porewater  $\text{Fe}^{2+}$  concentrations.<sup>32–34</sup> This is because the presence of higher porewater  $\text{Fe}^{2+}$  efficiently buffers porewater  $\text{H}_2\text{S}$  to very low concentrations and thereby minimizes sulfurization of organic matter. For this reason, As–thiol complexation is unlikely to have been a significant mechanism of As immobilization in the experiments described here.

Also, it is possible that As could have been immobilized via orpiment precipitation due to direct reaction between microbially-produced  $\text{H}_2\text{S}$  and porewater As. As discussed above, the presence of high porewater  $\text{Fe}^{2+}$  concentrations is expected to have efficiently removed  $\text{H}_2\text{S}$  from solution and thereby minimize direct interactions between porewater As and  $\text{H}_2\text{S}$ . From this perspective, we can consider porewater As and  $\text{Fe}^{2+}$  as competing for the limited supply of microbially-produced  $\text{H}_2\text{S}$ . This competition can be quantitatively evaluated by the following equilibrium reaction between  $\text{FeS}$  and  $\text{As}_2\text{S}_3$ :



where  $\log_{10} K = 33.9$ .<sup>20</sup> On the basis of this thermodynamic perspective,  $\text{FeS}$  would have outcompeted  $\text{As}_2\text{S}_3$  for the available  $\text{H}_2\text{S}$  due to the near-neutral pH conditions and the presence of very high porewater  $\text{Fe}^{2+}$  concentrations (Figure 7).

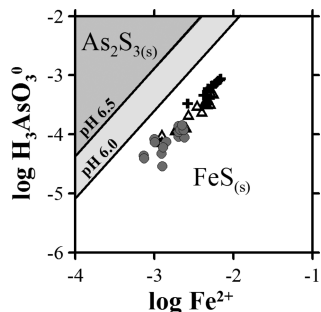


**Figure 7.** Relationship between aqueous As concentrations and aqueous Fe concentrations in the biotic treatments in relation to the fields of stability for  $\text{FeS}$  versus  $\text{As}_2\text{S}_3$ . Circles, triangles, and plus symbols denote the high, medium, and low sulfate treatments, respectively.

This is consistent with the presence of mackinawite in the biotic high  $\text{SO}_4^{2-}$  treatment and the corresponding absence of discrete orpiment crystals; hence, it is unlikely that precipitation of orpiment represented an important process in the experiments described here.

Finally, the observed decreases in As mobility under  $\text{SO}_4^{2-}$ -reducing conditions appear to have been caused by the sorption of As to mackinawite, which formed via the reaction between microbially-produced  $\text{H}_2\text{S}$  and  $\text{Fe}^{2+}$ . Although mackinawite has been proposed as an important sorbent for As in sulfidic systems,<sup>2,4,15,22–27,29</sup> direct microscopy-based evidence that

proves strong As–mackinawite interactions in natural soils has not been presented previously. The present study is therefore significant because the results provide direct evidence that confirms sorption of As to mackinawite during flooding of natural soil.

The finding of strong As enrichment within mackinawite differs from recent studies of model systems that show that mackinawite sorbed very little As in the presence of other Fe-rich sorbent phases.<sup>11–14</sup> These previous experiments all used relatively low aqueous As concentrations, which are in contrast to the very high aqueous As concentrations that developed as a result of microbial activity following flooding of the contaminated soil examined in the present study. The difference in observed As–mackinawite interactions between previous work and the present study probably reflects a change from complexation of As oxyanions at low loadings (as used in the previous studies<sup>11–14</sup>) to the development of much stronger As–S surface bonds at higher loadings (as occurred in the present study).<sup>25</sup>

Han et al.<sup>35</sup> found that, under mildly acidic conditions, As(III) was retained as an orpiment-like surface species in suspensions of mackinawite-coated sand. This earlier discovery, along with the HAADF-STEM results (Figure 7), suggests that the observed formation of an orpiment-like local coordination environment for As in the biotic high  $\text{SO}_4^{2-}$  treatment resulted from As complexation at the mackinawite surface as opposed to the precipitation of actual orpiment crystals. This type of surface complex (i.e., As–S species) differs significantly from the O-coordinated As species assumed to exist by Wolthers et al.<sup>24</sup> at the mackinawite–water interface. It also differs from the realgar-like species that have been observed in strongly reducing,  $\text{Fe}^{2+}$ -poor, mackinawite-bearing systems.<sup>18,19,25,26</sup> However, the formation of an orpiment-like surface complex on mackinawite supports earlier research into As behavior in an  $\text{Fe}^{2+}$ -rich system.<sup>15</sup>

**Environmental Implications.** Following flooding of As-contaminated soil, dissimilatory Fe(III)- and As(V)-reduction triggered the mobilization of substantial amounts of As into the aqueous phase. Under conditions where dissimilatory  $\text{SO}_4^{2-}$  reduction occurred to only a negligible or small degree, there was continued release of Fe and As from the solid-phase into the aqueous-phase over the full 10 week experiment duration. This supports earlier work that shows As mobilization as a result of As(V)-reduction and the reductive dissolution of Fe(III) oxyhydr(oxides) in flooded soil.<sup>4–6</sup> In contrast, after a lag of approximately 1 week, both Fe and As were partly retained by the solid phase in the presence of more substantial  $\text{SO}_4^{2-}$  reduction. The electron microscopy results suggest that this partial retention of Fe and As was a result of microbially mediated mackinawite formation.

Mackinawite has been hypothesized to be an important host-phase for As in sulfidic subsurface environments.<sup>2</sup> This is based largely on studies of As sorption to synthetic mackinawite, tightly constrained model experiments using a limited assemblage of mineral phases, or operationally defined extraction schemes.<sup>4,15,22–27,29</sup> However, direct microscopy-based observations that prove strong As–mackinawite interactions in natural soils or sediments have been previously lacking. The present study is the first to provide direct microscopy-based evidence that shows As sorption to mackinawite in natural soil.

## AUTHOR INFORMATION

### Corresponding Author

\*E-mail: ed.burton@scu.edu.au.

### Notes

The authors declare no competing financial interest.

## ACKNOWLEDGMENTS

Research expenses were provided by the Australian Research Council (ARC) under Grant No. DP110100519. Salary support for S.J. was provided by the ARC under Grant No. FT110100130. William Bennett and Jared Panther from Griffith University, Australia helped to collect the initial soil sample. The bulk XAS work was conducted at the Australian Synchrotron (Melbourne, Australia) with support from Chris Glover and Peter Kappen. The microfocussed XRF and XAS work was conducted at the Stanford Synchrotron Radiation Laboratory (SSRL; Menlo Park, CA). We thank Sam Webb for providing valuable advice and assistance during data collection at the SSRL. TEM was conducted at the University of Queensland (Brisbane, Australia) by Graeme Auchterlonie of the Centre for Microscopy and Microanalysis. SEM was conducted at Southern Cross University SEM laboratory with support from Maxine Dawes.

## REFERENCES

- (1) Smedley, P. L.; Kinniburgh, D. G. A review of the source, behaviour, and distribution of arsenic in natural waters. *Appl. Geochem.* **2002**, *17*, 517–568.
- (2) Charlet, L.; Morin, G.; Rose, J.; Wang, Y.; Auffan, M.; Burnol, A.; Fernandez-Martinez, A. Reactivity at (nano)particle-water interfaces, redox processes, and arsenic transport in the environment. *C. R. Geosci.* **2011**, *343*, 123–139.
- (3) Voegelin, A.; Weber, F.-A.; Kretzschmar, R. Distribution and speciation of arsenic around roots in a contaminated riparian floodplain soil: Micro-XRF element mapping and EXAFS spectroscopy. *Geochim. Cosmochim. Acta* **2007**, *71*, 5804–5820.
- (4) Burton, E. D.; Bush, R. T.; Sullivan, L. A.; Johnston, S. G.; Hocking, R. K. Mobility of arsenic and selected metals during re-flooding of iron- and organic-rich acid–sulfate soil. *Chem. Geol.* **2008**, *253*, 64–73.
- (5) Johnston, S. G.; Keene, A. F.; Burton, E. D.; Bush, R. T.; Sullivan, L. A.; McElnea, A. E.; Ahern, C. R.; Smith, C. D.; Powell, B. Arsenic mobilisation in a seawater inundated acid sulfate soil. *Environ. Sci. Technol.* **2010**, *44*, 2016–2021.
- (6) Weber, F.-A.; Hofacker, A. F.; Voegelin, A.; Kretzschmar, R. Temperature dependence and coupling of iron and arsenic reduction and release during flooding of a contaminated soil. *Environ. Sci. Technol.* **2009**, *44*, 116–122.
- (7) Parsons, C. T.; Couture, R.-M.; Omorogie, E. O.; Bardelli, F.; Greeneche, J.-M.; Roman-Ross, G.; Charlet, L. The impact of oscillating redox conditions: Arsenic immobilization in contaminated calcareous floodplain soils. *Environ. Pollut.* **2013**, *178*, 254–263.
- (8) Islam, F. S.; Gault, A. G.; Boothman, C.; Polya, D. A.; Charnock, J. M.; Chatterjee, D.; Lloyd, J. R. Role of metal-reducing bacteria in arsenic release from Bengal delta sediments. *Nature* **2004**, *430*, 68–71.
- (9) Keimowitz, A. R.; Mailloux, B. J.; Cole, P.; Stute, M.; Simpson, H. J.; Chillrud, S. N. Laboratory investigations of enhanced sulfate reduction as a groundwater arsenic remediation strategy. *Environ. Sci. Technol.* **2007**, *41*, 6718–6724.
- (10) Saalfeld, S. L.; Bostick, B. C. Changes in iron, sulfur, and arsenic speciation associated with bacterial sulfate reduction in ferrihydrite-rich systems. *Environ. Sci. Technol.* **2010**, *43*, 8787–8793.
- (11) Kirk, M. F.; Roden, E. E.; Crossey, L. J.; Bearley, A. J.; Spilde, M. N. Experimental analysis of arsenic precipitation during microbial sulfate and iron reduction in model aquifer sediment reactors. *Geochim. Cosmochim. Acta* **2010**, *74*, 2538–2555.
- (12) Kocar, B. D.; Borch, T.; Fendorf, S. Arsenic repartitioning during biogenic sulfidation and transformation of ferrihydrite. *Geochim. Cosmochim. Acta* **2010**, *74*, 980–994.
- (13) Burton, E. D.; Johnston, S. G.; Bush, R. T. Microbial sulfidogenesis in ferrihydrite-rich environments: Effects on iron mineralogy and arsenic mobility. *Geochim. Cosmochim. Acta* **2011**, *75*, 3072–3087.
- (14) Burton, E. D.; Johnston, S. G.; Planer-Friedrich, B. Coupling of arsenic mobility to sulfur transformations during microbial sulfate reduction in the presence and absence of humic acid. *Chem. Geol.* **2013**, *343*, 12–24.
- (15) Burton, E. D.; Johnston, S. G.; Kraal, P.; Bush, R. T.; Claff, S. Sulfate availability drives divergent evolution of arsenic speciation during microbially-mediated reductive transformation of schwertmannite. *Environ. Sci. Technol.* **2013**, *47*, 2221–2229.
- (16) Rochette, E. A.; Bostick, B. C.; Li, G. C.; Fendorf, S. Kinetics of arsenate reduction by dissolved sulfide. *Environ. Sci. Technol.* **2000**, *34*, 4714–4720.
- (17) Poulton, S. W.; Krom, M. D.; Raiswell, R. A revised scheme for the reactivity of iron (oxyhydr)oxide minerals towards dissolved sulfide. *Geochim. Cosmochim. Acta* **2004**, *68*, 3703–3715.
- (18) O'Day, P. A.; Vlassopoulos, D.; Root, R.; Rivera, N. The influence of sulfur and iron on dissolved arsenic concentrations in the shallow subsurface under changing redox conditions. *Proc. Natl. Acad. Sci. U.S.A.* **2004**, *38*, 13703–13708.
- (19) Root, R. A.; Vlassopoulos, D.; Rivera, N. A.; Rafferty, M. T.; Andrews, C.; O'Day, P. A. Speciation and natural attenuation of arsenic and iron in a tidally influenced shallow aquifer. *Geochim. Cosmochim. Acta* **2009**, *73*, 5528–5553.
- (20) Wilkin, R. T.; Ford, R. G. Arsenic solid-phase partitioning in reducing sediments of a contaminated wetland. *Chem. Geol.* **2006**, *228*, 156–174.
- (21) Johnston, S. G.; Burton, E. D.; Keene, A. F.; Planer-Friedrich, B.; Voegelin, A.; Blackford, M. G.; Lumpkin, G. R. Arsenic mobilisation and iron transformations during sulfidization of As(V)-bearing jarosite. *Chem. Geol.* **2012**, *334*, 9–24.
- (22) Bostick, B. C.; Fendorf, S. Arsenite sorption on troilite ( $\text{FeS}$ ) and pyrite ( $\text{FeS}_2$ ). *Geochim. Cosmochim. Acta* **2003**, *67*, 909–921.
- (23) Bostick, B. C.; Chen, C.; Fendorf, S. Arsenite retention mechanisms within estuarine sediments of pescadero, CA. *Environ. Sci. Technol.* **2004**, *38*, 3299–3304.
- (24) Wolthers, M.; Charlet, L.; van der Weijden, C. H.; van der Linde, P. R.; Rickard, D. Arsenic mobility in the ambient sulfidic environment: Sorption of arsenic(V) and arsenic(III) onto disordered mackinawite. *Geochim. Cosmochim. Acta* **2005**, *69*, 3483–3492.
- (25) Gallegos, T. J.; Han, Y.-S.; Hayes, K. F. Spectroscopic investigation of the uptake of arsenite from solution by synthetic mackinawite. *Environ. Sci. Technol.* **2007**, *41*, 7781–7786.
- (26) Renock, D.; Gallegos, T.; Utsunomiya, S.; Hayes, K.; Ewing, R. C.; Becker, U. Chemical and structural characterization of As immobilization by nanoparticles of mackinawite ( $\text{FeS}_m$ ). *Chem. Geol.* **2009**, *268*, 116–125.
- (27) Couture, R.-M.; Rose, J.; Kumar, N.; Mitchell, K.; Wallschlager, D.; Van Cappellen, P. Sorption of arsenite, arsenate, and thioarsenates to iron oxides and iron sulfides: A kinetic and spectroscopic investigation. *Environ. Sci. Technol.* **2013**, *47*, 5652–5659.
- (28) Niazi, N. K.; Singh, B.; Shah, P. Arsenic speciation and phytoavailability in contaminated soils using a sequential extraction procedure and XANES spectroscopy. *Environ. Sci. Technol.* **2011**, *45*, 7135–7142.
- (29) Paul, C. J.; Ford, R. G.; Wilkin, R. T. Assessing the selectivity of extractant solutions for recovering labile arsenic associated with iron (hydr)oxides and sulfides in sediments. *Geoderma* **2009**, *152*, 137–144.
- (30) Ravel, B.; Newville, M. ATHENA, ARTEMIS, HEPHAESTUS: Data analysis for X-ray absorption spectroscopy using IFEFFIT. *J. Synchrotron. Rad.* **2005**, *12*, 537–541.

- (31) USEPA. National primary drinking water regulations; Arsenic and clarifications to compliance and new source contaminants monitoring; Final rule. *Fed. Regist.* **2001**, *66* (14), 6697–7066.
- (32) Couture, R.-M.; Wallschläger, D.; Rose, J.; Van Cappellen, P. Arsenic binding to organic and inorganic sulfur species during microbial sulfate reduction: A sediment flow-through reactor experiment. *Environ. Chem.* **2013**, *10*, 285–294.
- (33) Langner, P.; Mikutta, C.; Kretzschmar, R. Arsenic sequestration by organic sulfur in peat. *Nat. Geosci.* **2012**, *5*, 66–73.
- (34) Langner, P.; Mikutta, C.; Suess, E.; Marcus, M. A.; Kretzschmar, R. Micro-scale distribution and speciation of arsenic in peat studied with microfocused X-ray fluorescence spectrometry and X-ray absorption spectroscopy. *Environ. Sci. Technol.* **2013**, *47* (17), 9706–9714.
- (35) Han, Y.-S.; Jeong, H. Y.; Demond, A. H.; Hayes, K. F. X-ray absorption and photoelectron spectroscopic study of the association of As(III) with nanoparticulate FeS and FeS-coated sand. *Water Res.* **2011**, *45*, 5727–5735.